Available online at www.sciencedirect.com
SCIENCE DIRECT
Polymer 46 (2005) 11624–11634
polymer
www.elsevier.com/locate/polymer

Micro- and nano-structure in polypropylene/clay nanocomposites

F. Perrin-Sarazin *, M.-T. Ton-That, M.N. Bureau, J. Denault

Industrial Materials Institute, National Research Council of Canada, 75, de Mortagne, Boucherville, Que., Canada J4B 6Y4

Received 3 November 2004; received in revised form 22 September 2005; accepted 24 September 2005
Available online 24 October 2005

Abstract

Polypropylene (PP)/clay nanocomposites prepared by melt blending using different clays and coupling agents based on maleic anhydride-grafted PP (MA-PP) were studied. Clay dispersion using field emission gun scanning electron microscope (FEG-SEM) and transmission electron microscopy (TEM), and PP matrix morphology were characterized. Clay dispersion was improved in the presence of MA-PP, as shown by the higher particles surface density (number of particles/mm^2) at all micro-, sub-micro- and nano-levels. The PP spherulite diameter was affected by both the presence of MA-PP and clay dispersion. Clay intercalation, characterized by both complementary X-ray diffraction (XRD) and TEM, was greatly influenced by the characteristics of MA-PP. The use of low molecular weight (M_w) MA-PP led to a good and uniform intercalation but with no further possibility to exfoliation. The use of higher M_w MA-PP led to a heterogeneous intercalation with signs of exfoliation. The crystallization behavior of nanocomposites was studied by differential scanning calorimetry (DSC). When fine clay dispersion was achieved with MA-PP, clay-nucleating effect was limited and lower crystallization temperature and rates were observed. It was also shown by wide angle X-ray diffraction (WAXD) that clay induced some orientation of α-phase PP crystallites.

Keywords: Polymer nanocomposites; Microstructure; Clay dispersion

1. Introduction

Polymer nanocomposites (PNCs) are a new kind of composite materials in which the reinforcement has at least one nanometric dimension. Among the range of nano-reinforcements used in PNCs, clays have been widely studied because of their potential to exfoliate in the polymer matrix as single nanometric platelets leading to markedly superior mechanical properties, improved flammability resistance and barrier properties at low cost [1].

PNCs are now prepared by different methods, namely in situ polymerization, solvent process and melt compounding. PNCs are also made using a large variety of thermosetting and thermoplastic polymers [2]. From an industrial point of view, preparation of thermoplastic PNCs by melt blending using conventional plastic compounding tools remains the solution of choice, especially with commodity resins like PP, which is of great interest for the automotive industry. However, melt blended PP-based nanocomposites remain an important challenge since complete exfoliation, i.e. the dispersion of clay in single platelets, has not yet been successfully achieved. Most of the developed formulations have shown a relatively limited intercalation, i.e. the clay particles still consisting of well aligned, ordered distanced platelets. The use of coupling agents mainly based on MA-PP has been shown to significantly improve clay intercalation depending on their characteristics as molecular weight and grafting content [3–5] and on the coupling agent-to-clay ratio [3,6,7]. Intercalation was also shown to be affected by the type and content of clay [8–10] and the type of clay intercalant, i.e. clay organic modification [11]. In general, improved intercalation is obtained at relatively low clay content and high coupling agent-to-clay ratio.

It is also known that in semi-crystalline PP-based nanocomposites the addition of coupling agent can greatly affect the matrix morphology and usually leads to good clay intercalation instead of exfoliation. In such a case, the microstructural characterization in terms of matrix morphology and clay dispersion at both the micro- and nano-level becomes crucial to understand the effect of the formulation on the resulting PNCs properties. In the literature, the emphasis has been put on the characterization of clay dispersion and intercalation at a nano-level using TEM and XRD techniques, but information is often missing concerning the morphology at the micro-level, especially in the case of intercalated PNCs in which clays are still organized in stacked platelets forming micron-sized particles that will have impact on matrix

* Corresponding author. Tel.: +450 641 5145; fax: +450 641 5105.
E-mail address: florence.perrin@imi.cnrc-nrc.gc.ca (F. Perrin-Sarazin).

0032-3861/$ - see front matter © 2005 Elsevier Ltd. All rights reserved.
doi:10.1016/j.polymer.2005.09.076

crystallization and mechanical properties. Therefore, the objective of this work is to better understand the influence of different MA-PP coupling agents and organo-modified clays on the clay dispersion and intercalation and on the matrix morphology, by studying the microstructure of PP-based nanocomposites at both the micro- and nano-level and the crystallization behavior of the matrix.

2. Experimental

2.1. Materials and preparation

The PP matrix used was a homopolymer Pro-fax PDC 1274 (M_w = 250 kg/mol) from Basell. Two types of MA-PP were used as coupling agents: a low M_w and high grafting content, Epolene E43 (M_w = 9.1 kg/mol, MA content: 3.8%) from Eastman Chemical, chosen for its expected better interaction with clay, and a high M_w and low grafting content, Polybond 3150 (M_w = 330 kg/mol, MA content: 0.5%) from Crompton Co., chosen for its expected better miscibility with the PP matrix. These two coupling agents are identified as MA9k and MA330k respectively. Two types of organo-modified montmorillonite were used as clay reinforcements: Cloisite 15A (intercalant: quaternary ammonium salt; intercalant content: 125 meq/100 g; interlayer spacing: d_{001} = 3.15 nm) and Cloisite 30B (intercalant: quaternary ammonium salt; intercalant content: 90 meq/100 g; interlayer spacing: d_{001} = 1.85 nm) from southern clay products. These clays are identified as 15A and 30B respectively.

Blends of PP and MA-PP without clay and nanocomposites with and without MA-PP were compounded in a twin-screw extruder Leistritz (L/D = 34 mm) at a temperature of 200 °C. To better control the clay content in the nanocomposites, some of the formulations were prepared from a masterbatch of PP and 10 wt% clay. All formulations prepared are described in Table 1. For characterization, nanocomposites and polymer blend samples were molded by compression in a Carver press at 200 °C. The thickness of the samples was 0.8 mm.

2.2. Characterization of the clay dispersion and matrix morphology

2.2.1. Microscopy

SEM characterization of the polymer blends and nanocomposites was done on polished and chemically etched sample cross-section using low voltage FEG-SEM Hitachi S-4700 after coating with a vapor deposit of platinum. Chemical etching was done using a solution of 0.7 wt%/v potassium permanganate in a 2:1 mixture of sulphuric and orthophosphoric acids, following a procedure which was optimized for the PP nanocomposites from the basic method described by Olley and Bassett [12].

TEM characterization of the nanocomposites was done on cryo-ultramicrotomed sections using high resolution microscope Hitachi H 9000 operating at 300 kV.

Image analysis of the micrographs was done to determine the equivalent spherulite diameter and clay particle length. Clay dispersion was quantified from the clay particles surface density, i.e. the number of clay particles per unit surface, at a magification of 3500× where only clay particles longer than 1 μm were counted, and at a magnification of 15,000×, where only clay particles smaller than 1 μm were counted. These magnification levels are henceforth referred to as micro-level and sub-micro-level respectively. Clay dispersion was also characterized from TEM micrographs at such a sub-micro level and at a nano-level too. For the latter, the analysis results done at a magnification of 80,000× where only clay particles having less than three platelets were counted, should be considered as semi-quantitative due to the low number of particles counted.

2.2.2. X-ray diffraction

X-ray diffraction was done at small angles to determine the degree of clay intercalation and at wide angles to characterize the PP crystalline phases. In both cases, a Bruker Discover 8 diffractometer operating at 40 kV, 40 mA with Cu K_α radiation in reflection mode using a horizontal Bragg–Brentano focusing geometry was used. Analysis of the XRD patterns was done using basic peak fitting with Pearson VII function after background subtraction.

Following the Scherrer equation [13], the mean crystallite size, L, in the direction perpendicular to the (hkl) plane was determined following:

Table 1
Blends and nanocomposites formulations

Formulations	Clays		Coupling agents		Compounding
	15A	30B	MA9k	MA330k	
PP					Direct
PP/MA9k			4 wt%		Direct
PP/MA330k				4 wt%	Direct
PP/15A	2 wt%				Direct
PP/15A/MA9k	2 wt%		4 wt%		Direct
PP/15A/MA330k	2 wt%			4 wt%	Direct
m(PP/15A)/MA330k	2 wt%			4 wt%	From masterbatch
m(PP/30B)/MA330k		2 wt%		4 wt%	From masterbatch

$$L_{hkl} = \frac{K\lambda}{B\cos\theta_{hkl}} \quad (1)$$

where K is the crystallite shape constant ($=0.89$), λ is the wavelength of Cu K_α radiation (1.540598 Å), $B = (b_{hkl}^2 - b_0^2)^{1/2}$, where b_{hkl} is the full width middle height (FWMH) of the peak for the (hkl) reflection and b_0 the instrumental resolution determined from the LaB_6 reference sample, and is the diffraction angle. Eq. (1) was used to express the PP crystallite size, L_{040}, perpendicular to the (040) plane and the mean clay particle size, t, perpendicular to the (001) plane corresponding to the clay platelet surface. From the latter, the number of platelets per clay particles was calculated following [14]:

$$N = \frac{t + d_{001} - d_p}{d_{001}} \quad (2)$$

where N is the number of clay platelets, d_p is the thickness of one single platelet ($=1$ nm) and d_{001} is the clay interlayer spacing, i.e. distance between two adjacent clay platelets, determined from the Bragg's law ($\lambda = 2d_{001}\sin\theta_{001}$).

From wide angle X-ray diffraction (WAXD) pattern, the PP α-phase orientation indexes were determined following [15]:

$$A_{110} = \frac{h_{\alpha_1}}{h_{\alpha_1} + h_{\alpha_4}} \quad (3)$$

$$A_{040} = \frac{h_{\alpha_2}}{h_{\alpha_1} + h_{\alpha_2} + h_{\alpha_3}} \quad (4)$$

where h is the peak height after background subtraction, α_1 corresponds to the (110) reflection, α_2 to the (040) reflection, α_3 to (130) reflection and α_4 to the (111) and ($\bar{1}31$)(041) reflections. The A_{110} index is based on the extinction of ($hk1$) reflections (in which case, A_{110} tends to 1) relatively to the (110) reflections. It thus gives an indication of an orientation roughly parallel to the c-axis of the crystallites corresponding to the flow direction in injected samples [16]. The A_{040} index is based on the extinction of the (hk0) reflections relatively to the (0k0) reflections and gives an indication of a preferential orientation perpendicular to the b-axis of the crystallites, i.e. pretty much parallel to the surface sample [16].

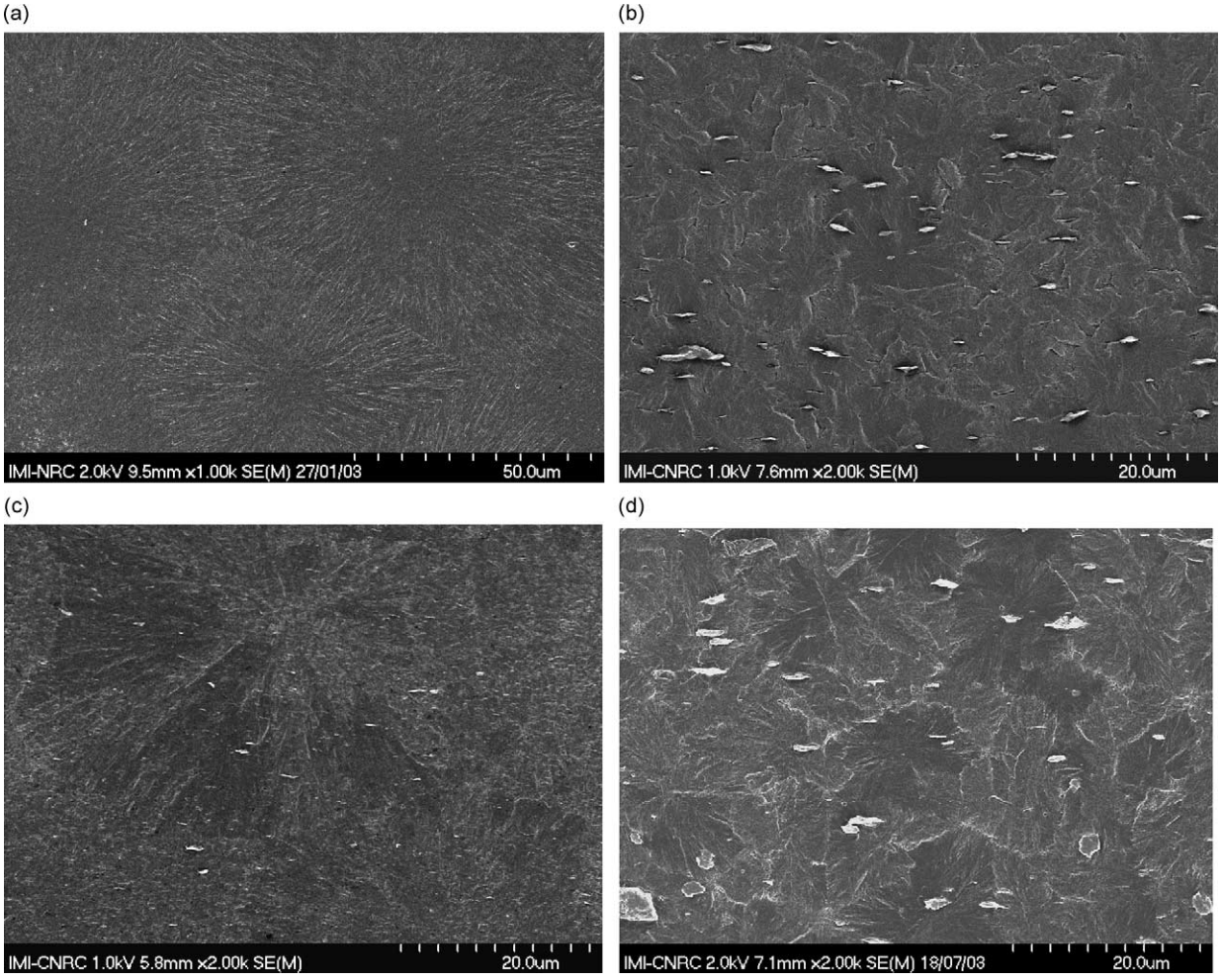

Fig. 1. Typical FEG-SEM micrographs (a) PP, (b) PP/15A, (c) PP/15A/MA330k and (d) m(PP/30B)/MA330k after surface etching.

Note that, instead of A_{110} from Eq. (3), a more general index, A_{hk0}, given by Eq. (5) is reported in this work since the validity of the A_{110} index based on a constant ratio $h_{\alpha_3}/h_{\alpha_1}$ [15] was not observed in our samples.

$$A_{hk0} = \frac{h_{\alpha_1} + h_{\alpha_2} + h_{\alpha_3}}{h_{\alpha_1} + h_{\alpha_2} + h_{\alpha_3} + h_{\alpha_4}} \tag{5}$$

A crystallinity index expressed as follows was also determined for comparison purpose [15]:

$$C_i = h_{\alpha_1} + h_{\alpha_2} + h_{\alpha_3} + h_{\alpha_4} \tag{6}$$

where C is the crystallinity index and i designates the studied condition.

2.2.3. Differential scanning calorimetry

The crystallization behavior of polymer blends and nanocomposites was studied using a DSC-7 Perkin–Elmer calorimeter at a cooling rate of 20 °C/min. The crystallinity of the PP matrix in the materials was determined as follows:

$$\chi = \frac{\Delta H_m}{f_p \Delta H_f^0} \times 100 \tag{7}$$

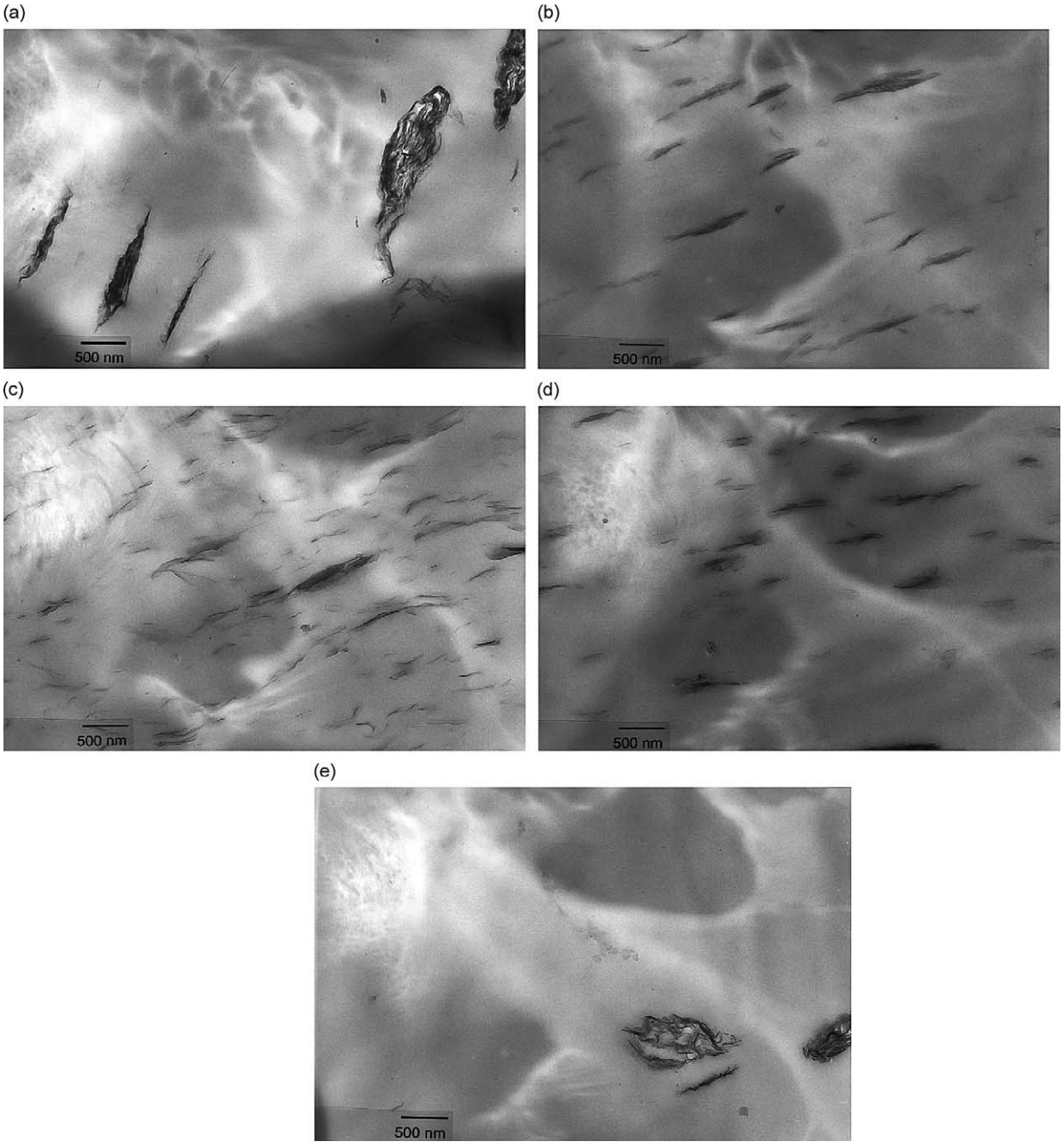

Fig. 2. TEM micrographs of nanocomposites at magnification of 15,000× (a) PP/15A, (b) PP/15A/MA9k, (c) PP/15A/MA330k, (d) m(PP/15A)/MA330k and (e) m(PP/30B)/MA330k.

where ΔH_m (J/g) is the enthalpy of melting of the polymer matrix, f_p is the PP weight fraction in the sample and ΔH_f^0 is the enthalpy of melting of pure crystalline PP (207.1 J/g [17]).

3. Results and discussion

3.1. PP morphology and clay dispersion

The dispersion of clay particles and the crystalline morphology of the PP matrix in both PP/MA-PP blends and nanocomposites were observed on FEG-SEM micrographs of etched samples and from TEM observations. Typical examples of these micrographs are shown in Figs. 1 and 2. As shown in Fig. 1(a), chemical etching revealed large spherulites in the PP matrix. With the addition of clay 15A in pure PP, a strong spherulite size reduction is obtained (Fig. 1(b)) while with the presence of the coupling agents (MA9k and MA330k) such a reduction is not observed (Fig. 1(c)). However, in the cases of samples prepared from the masterbatch, m(PP/15A)/MA330k and m(PP/30B)/MA330k, a certain spherulite size reduction is observed (Fig. 1(d)). Coarse clay dispersion is observed in PP/15A by both FEG-SEM (Fig. 1(b)) and TEM (Fig. 2(a)) whereas fine clay dispersion is obtained when adding the two coupling agents (Figs. 1(c) and 2(b)–(d)). In the case of PP/15A/MA330k, TEM observations (Fig. 2(c)) reveal the presence of very small size particles, not observed in the other nanocomposites. Despite the presence of coupling agent in m(PP/30B)/MA330k, a similar coarse clay dispersion to that for PP/15A is observed at both FEG-SEM (Fig. 1(d)) and TEM (Fig. 2(e)).

In order to obtain a quantification of the PP morphology and clay dispersion, image analysis was performed at different magnification levels. The spherulite diameter, clay particle length and clay surface density are reported in Table 2. The results of these analysis show that the presence of coupling agent affects the crystalline morphology of PP by reducing the average spherulite diameter by more than 50%. This reduction is more pronounced for PP/MA330k than for PP/MA9k. The standard deviation associated with the value of the average spherulite diameter is also considerably smaller for PP/MA330k. Such a difference observed between these two materials could be attributed to their very different molecular weight and grafting content [18]. When adding clay, the spherulite diameter is drastically reduced from 79 μm for PP to 8 μm for PP/15A. However, adding a coupling agent to PP/clay system (PP/15A/MA9k and PP/15A/MA330k) does not lead to such a reduction, but an increase of the spherulite diameter to 65 and 35 μm, respectively, that is higher in comparison with the PP/MA9k and PP/MA330k blends. However, the nanocomposites made from the masterbatch (m(PP/15A)/MA330k and m(PP/30B)/MA330k) both show similar spherulite size reduction to diameters of about 12 μm.

Results from Table 2 show that the average clay particle length in the nanocomposites is greatly reduced in the presence of the coupling agent. For all PP/15A/MA9k, PP/15A/MA330k and m(PP/15A)/MA330k a similar average clay particle length, less than half of that in PP/15A, is obtained. Despite the presence of coupling agent in m(PP/30B)/MA330k, large average clay particle length of more than 1 μm is obtained as for PP/15A. As expected, results of clay surface density determined from FEG-SEM micrographs show that PP/15A presents the highest density of micro-level particles (30×10^3/mm^2) and a low density of sub-micro-level particles (17×10^3/mm^2). This is in agreement with the large average particle length measured (1.88 μm) and the relatively large clay particle thickness observed in PP/15A (Fig. 1(b)). Relatively high density of micro-level particles (12×10^3/mm^2) and low density of sub-micro-level particles are observed for m(PP/30B)/MA330k that also shows large particle length (1.62 μm). The thicker clay particles observed in this nanocomposite (Fig. 1(d)) can explain the lower clay densities measured at both levels compared to PP/15A. For the PP/15A/MA9k, PP/15A/MA330k and m(PP/15A)/MA330k, similar low density of micro-level particles (less than 10×10^3/mm^2) and very high density of sub-micro-level particles (more than 400×10^3/mm^2) are obtained. This is also in agreement with the small average clay particle length determined in these nanocomposites. Clay surface densities determined from TEM at a sub-micro-level show the same trend than from FEG-SEM except

Table 2
Microstructural parameters from quantitative image analysis

	Average spherulite diameter (μm)	Average clay particle length (μm)	Clay surface density (number of clay particles per mm$^2\times10^3$)			
			FEG-SEM		TEM	
			Micro-level (clay ≥ 1 μm)	Sub-micro-level (clay < 1 μm)	Sub-micro-level (clay < 1 μm))	Nano-level (3 platelets ≤)
PP	79 ± 10	–		–		
PP/MA9k	46 ± 8	–		–		
PP/MA330k	28 ± 1	–		–		
PP/15A	8 ± 1	1.88 ± 0.29	30 ± 5	17 ± 9	57 ± 25	
PP/15A/MA9k	65 ± 9	0.70 ± 0.06	4 ± 2	428 ± 53	1239 ± 149	
PP/15A/MA330k	35 ± 5	0.65 ± 0.07	8 ± 2	458 ± 134	2908 ± 372	8692 ± 2506
m(PP/15A)/MA330k	12 ± 1	0.56 ± 0.04	5 ± 2	502 ± 53	1511 ± 244	
m(PP/30B)/MA330k	14 ± 2	1.62 ± 0.34	12 ± 6	11 ± 9	32 ± 41	

that for PP/15A/MA330k where a significant higher density of sub-micro-level particles ($2908 \times 10^3/mm^2$) is obtained. This is explained by the presence of nano-level clay particles consisted of two or three platelets observed in this condition only (Fig. 2(c)) and whose density was determined around $8692 \times 10^3/mm^2$.

From the microscopic observations and their quantitative analysis, it can be seen that without coupling agent, clay dispersion in PP/15A is coarse showing large particles with high micro-level density but low sub-micro-level density. Since, no coupling agent is added, clay particles dispersion in PP/15A only results from the compounding process, which led to a micro-composite with micron-sized particles. In general, adding a coupling agent greatly improves clay dispersion by acting as a good dispersant during compounding. Fine clay dispersion characterized by small clay length, low micro-level clay density and high sub-micro-level clay density, is obtained in nanocomposites with clay 15A in the presence of the two coupling agents used. With coupling agent MA330k, the presence of numerous particles at both micro-level and nano-level suggests that clay dispersion in this nanocomposite is less homogeneous than that made with MA9k. With the presence of coupling agents in these nanocomposites, no spherulite size reduction is observed, except for the one made from the masterbatch process. The additional thermal/compounding history caused by the masterbatch process could probably affect the crystallization behavior of the PP. Despite the presence of the coupling agent in the nanocomposite with clay 30B prepared from the masterbatch process, the very poor clay dispersion observed indicates that the dispersant effect of MA330k is strongly limited and that clay aggregation takes place. As shown in a previous study [19], clay 30B presents lower thermal stability compared to clay 15A, showing signs of degradation below 200 °C. The lower degradation temperature of the intercalant in clay 30B probably contributes to the clay platelets collapse during the compounding and to the increase of the clay surface tension, leading to stronger platelet-to-platelet and particle-to-particle interactions responsible for clay aggregation.

3.2. Clay intercalation

The level of intercalation in clay powders and nanocomposites was determined by the measurement of the clay interlayer spacing (d_{001}) from the 2θ position of the clay (001) diffraction peak using Bragg's law. The X-ray diffraction patterns obtained are presented in Fig. 3(a). Peak fitting analysis was done using the Pearson VII function. An example of the peak fitting results is shown in Fig. 3(b). The results of this analysis are reported in Table 3.

As shown in Fig. 3(a), natural montmorillonite clay shows a diffraction peak at $2\theta = 7.3°$, which corresponds to an interlayer spacing of 1.2 nm. Peak fitting analysis for organo-modified clays (clays 15A and 30B) shows the presence of a low intensity peak at the same angle (peak 3 in Table 3), but also reveals the presence of two higher intensity peaks at lower angles (peaks 1 and 2 in Table 3). The organic modification

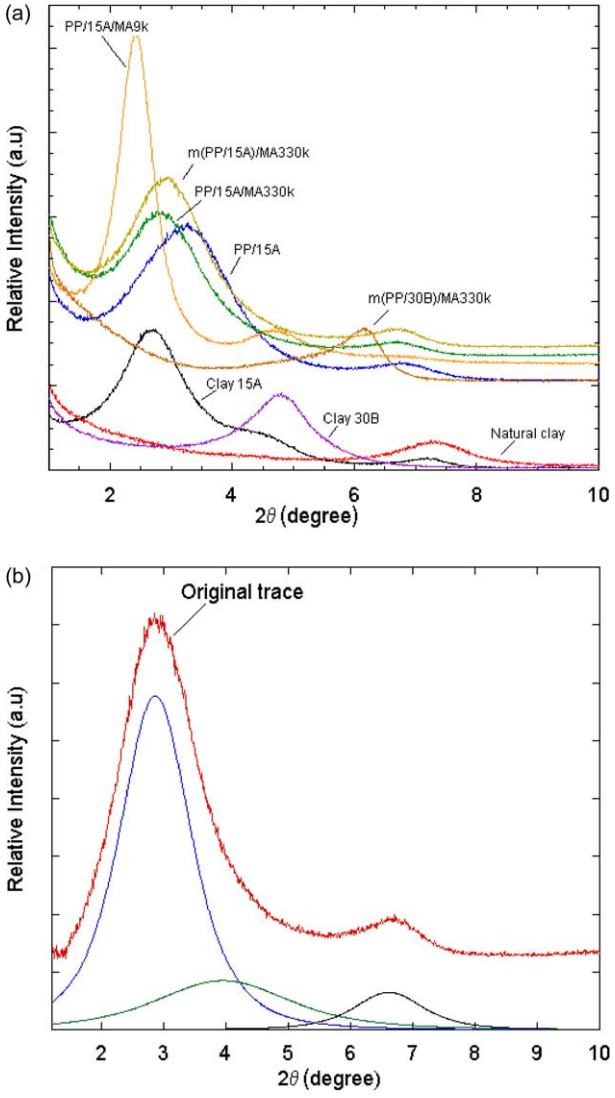

Fig. 3. XRD patterns (a) original traces for all clays and nanocomposites and (b) example of peak fitting.

thus leads to, as expected, an increase of the interlayer spacing due to the presence of the intercalant between the clay platelets but also to a wider distribution of the interlayer spacing. In agreement with the technical information provided by the clay suppliers, the highest intensity peak is, for clay 15A, located at lower angle than for clay 30B thus indicating that higher clay intercalation is achieved in 15A ($d_{001} = 3.3$ nm) compared to 30B ($d_{001} = 1.8$ nm).

In PP/15A, the highest intensity peak is shifted to higher angle compared to that of clay 15A suggesting that the interlayer spacing of clay 15A tends to decrease once processed in the polymer. Low thermal stability of the clay intercalant leading to clay collapse during compounding may be responsible for this interlayer spacing reduction. Such phenomenon is greatly reduced when a coupling agent is used in the nanocomposites showing that despite the probable intercalant degradation, the presence of coupling agent plays an important role on the intercalation. This is the case for PP/15A/MA9k, PP/15A/MA330k and m(PP/15A)/MA330k for

Table 3
Features from XRD patterns

	From peak fitting					
	Interlayer d_{001} spacing (nm) (intensity %)			FWHM (deg) of the 100%-intensity peak	Mean particle size t (nm) (from Eq. (1))	Number of platelets per particle (from Eq. (2))
	From peak 1	From peak 2	From peak 3			
Natural montmorillonite			1.2 (100%)	1.3		
Clay 15A	3.3 (100%)	2.0 (23%)	1.2 (8%)	1.2		
Clay 30B	2.3 (20%)	1.8 (100%)	1.5 (8%)	1.0		
PP/15A	3.3 (23%)	2.6 (100%)	1.3 (11%)	1.4	5.5	2.7
PP/15A/MA9k	3.6 (100%)	1.9 (10%)	1.3 (2%)	0.6	12.7	4.2
PP/15A/MA330k	3.1 (100%)	2.2 (15%)	1.3 (11%)	1.3	6.0	2.6
m(PP/15A)/MA330k	3.0 (100%)	2.1 (11%)	1.3 (12%)	1.4	5.5	2.5
m(PP/30B)/MA330k	1.8 (41%)	1.5 (44%)	1.4 (100%)	0.5	15	10.8

which the interlayer spacing determined from the highest intensity peak is above 3.0 nm, higher than for PP/15A (Table 3). However, as shown by Fig. 3(a), their peak shape is quite different. An intense and sharp peak (FWHM = 0.6°) is observed at relatively small angles for PP/15A/MA9k whereas a smaller and broader peak (FWHM = 1.4°) shifted between PP/15A and the latter is observed for both PP/15A/MA330k and m(PP/15A)/MA330k. The presence of this broad peak suggests a wider distribution (i.e. range) of interlayer spacing probably related to a more heterogeneous intercalation. The relative high intensity of peak 3 obtained for these nanocomposites (Table 3) suggests that less clay seems to undergo intercalation. However for PP/15A/MA330k, the presence of nano-level particles observed by TEM (Fig. 2(c)) suggests that intercalation probably occurred to a different extent.

High magnification TEM micrographs presented in Fig. 4 stress the difference observed between PP/15A/MA9k and PP/15A/MA330k. In PP/15A/MA9k, clay particles consist of well aligned and regularly spaced platelets, as shown in Fig. 4(a) and (b). On the contrary, particles in PP/15A/MA330k show a wider range of alignment and order, from well aligned ordered platelets to disordered platelets, as shown in Fig. 4(c) and (d). Small particles of 2–3 platelets are also often observed in PP/15A/MA330k, such as in Fig. 4(e), whereas such particles are not observed in PP/15A/MA9k. Also, the interlayer spacing of the less-ordered particles in Fig. 4(c) and (d) is significantly greater than in ordered particles. Irregularity in the interlayer spacing to larger distance is considered to be the effect of the penetration of PP into the interlayer spacing of the particles that eventually occurs and leads to the formation of small 2–3 platelets thick particles. These TEM observations thus complement XRD results and provide an explanation to the origin of the clay peak broadening observed in PP/15A/MA330k. The average peak value of the XRD curve from which the interlayer spacing is calculated is lower for PP/15A/MA330k (d_{001} = 3.1 nm) than for PP/15A/MA9k (d_{001} = 3.6 nm) but it takes into account a wider range of intercalated particles, from almost exfoliated (2–3 platelets thick) to non-intercalated particles. However, as shown by TEM observations, higher level of intercalation for some clay particles is achieved in this condition. These results emphasize the importance of using complementary techniques like TEM and XRD since XRD gives a large volume but intensity-proportional characterization limited to d-spacing determination below 10 nm and TEM gives a small volume characterization but with a whole representation of the materials.

The pattern obtained for m(PP/30B)/MA330k (Fig. 3(a)), shows that the highest intensity peak is shifted at higher angles compared to that of clay 30B, despite the presence of coupling agent in this nanocomposite. Peak positions and intensities reported for m(PP/30B)/MA330k in Table 3 comparatively to clay 30B, confirm that clay platelets collapse, instead of intercalation, occurred. This result is probably due to the smaller initial interlayer spacing of clay 30B compared to clay 15A and also to its low thermal stability.

Clay particle size, i.e. thickness, was determined from the peak broadening according to the Scherrer equation (Eq. (1)) and results are reported in Table 3. The clay particle size and number of platelets per particle determined are not in agreement with the TEM observations. Such results are not surprising considering that only quite small clay particles (considered less than 200 nm) actually contribute to the diffraction peak broadening, which can lead to contradictory results especially in the case of PP/15A. Moreover, the assumptions of perfect lattice and absence of strain effect, used in the Scherrer equation, are hardly verified in natural clay [20]. This, combined with clay collapse and intercalation effects inducing additional non-negligible strain effects as well as interlayer spacing distribution, makes the straightforward application of the Scherrer equation quite difficult.

3.3. Matrix crystallization and phase orientation

The overall crystallization behavior of the polymer blends and nanocomposites is presented in Fig. 5 by the cooling curves and the transformation curves representing the area under the crystallization peak in percent as a function of the temperature. The position and the slope of such curves are an indication of the crystallization temperature range and crystallization rate respectively. As shown in Fig. 5, the PP/MA9k blend presents a similar crystallization behavior than the PP whereas the PP/MA330k blend shows higher crystallization temperature and

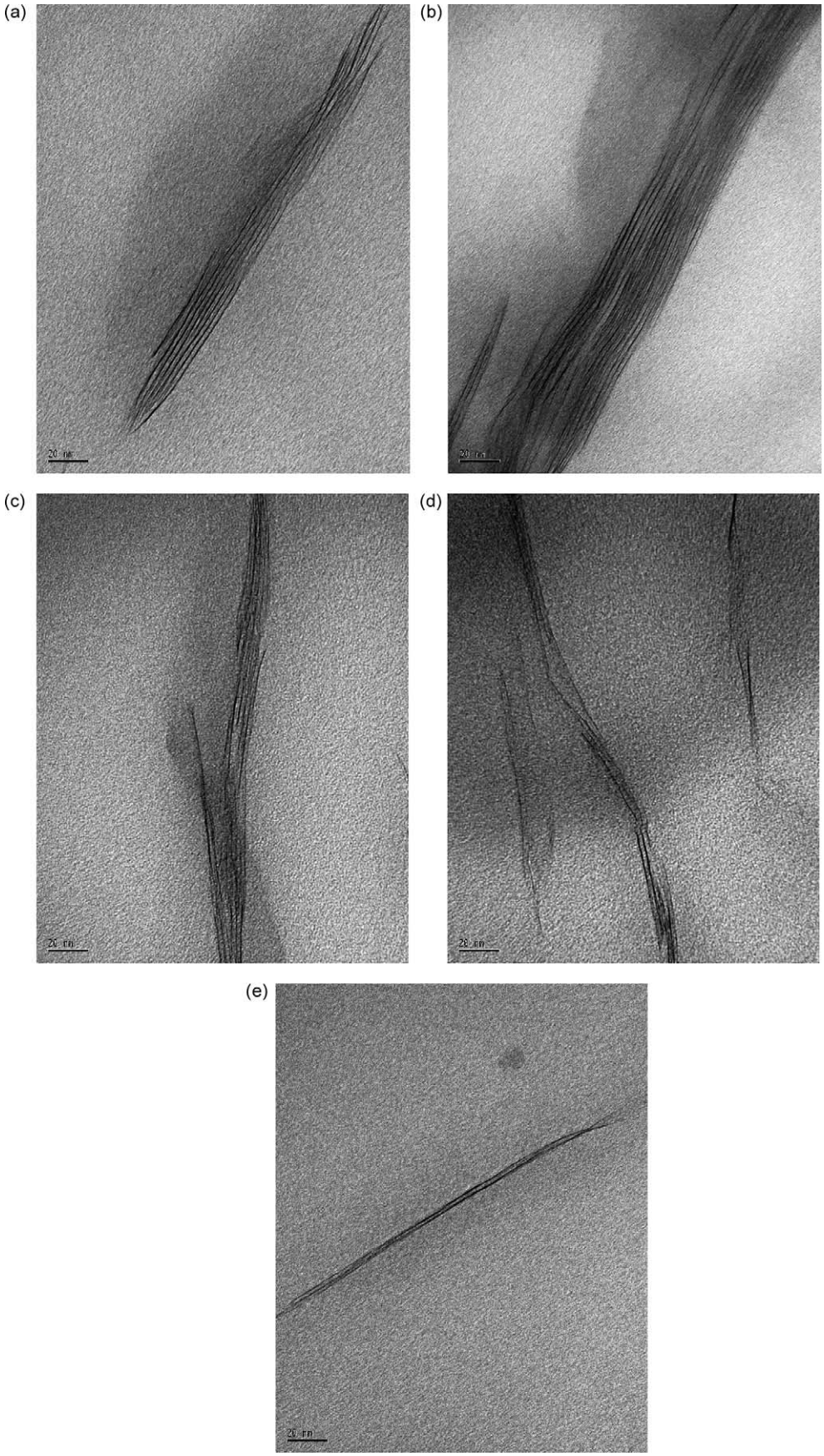

Fig. 4. TEM micrographs of PP/15A/MA9k: (a) and (b); and PP/15A/MA330k: (c), (d) and (e) and magnification of 500,000×.

rate. The PP/15A nanocomposite also shows a higher crystallization temperature and the highest crystallization rate obtained among the materials tested. For the PP/15A/MA9k and PP/15A/MA330k nanocomposites, however, the crystallization occurs at much lower crystallization rates and at temperatures only slightly above that of the pure PP. For the m(PP/15A)/MA330k and m(PP/30B)/MA330k nanocomposites, the crystallization rates are similar to the PP/15A/MA9k and PP/15A/MA330k, but the crystallization temperatures remained higher.

These results show that the crystallization of PP is significantly affected by both the presence of coupling agent and clay. In the blends without clay, the presence of the coupling agent, despite its relatively low content (4 wt%), causes the crystallization of PP to occur at higher temperature and higher rates. These effects on the crystallization are in agreement with the importance of the spherulite size reduction (Table 2), more pronounced when MA330k is used instead of MA9k. Clay addition, at least when no coupling agent is used, has a similar but more marked effect on the crystallization behavior. In the latter, where no favorable PP-clay interactions exist, conventional heterogeneous nucleation effects are observed, in agreement with pronounced reduction in spherulite size in the PP/15A (Table 2). When a coupling agent is added in the nanocomposites, the crystallization behavior tends to be much more similar to PP, in agreement again with the weaker reductions in spherulite size compared to the respective blend (Table 2). These results thus suggest that the PP-clay interface plays an important role in the crystallization behavior, with specific PP-clay interactions involving probably MA groups of the coupling agent that limit the nucleating effect of the clay particles [21]. The nanocomposites made from masterbatch seem to show similar low crystallization rate as for nanocomposites made from direct process but show higher crystallization temperature. This is in agreement with the relative smaller spherulite size observed (Table 2). This result could be due to the different mechanical flow and thermal histories induced by the masterbatch process and affecting the PP-clay interface by the thermal degradation of the intercalant. While the crystalline morphology of PP in the polymer blends and the nanocomposites is affected by their formulation, the level of crystallinity however is very similar for all materials studied, with all results comprised between 41 and 44%.

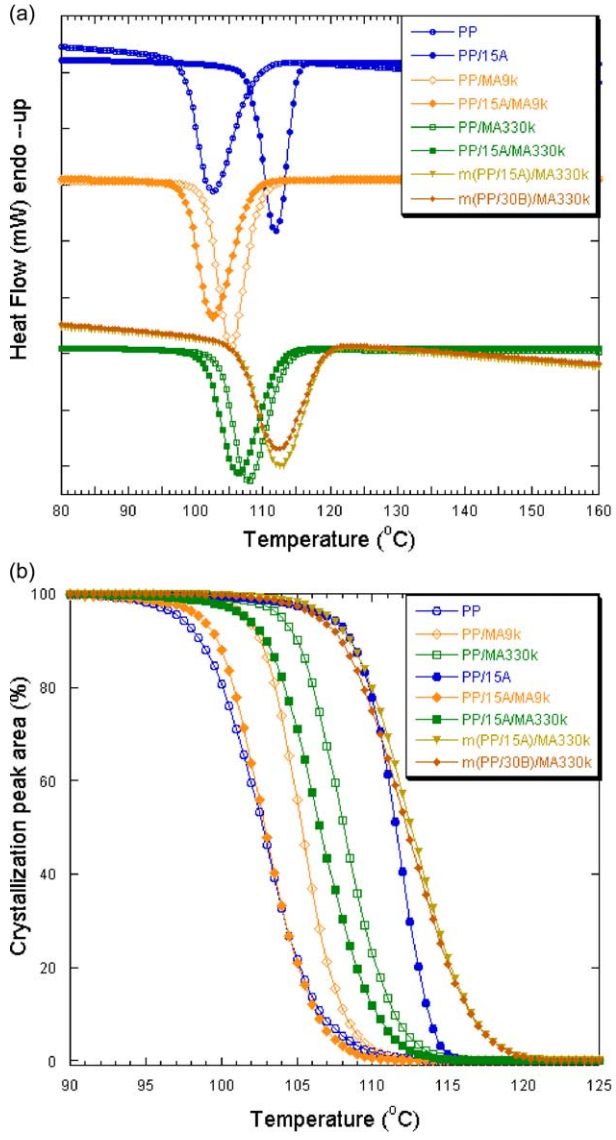

Fig. 5. DSC curves of blends and nanocomposites (a) cooling scans and (b) transformation curves.

WAXD patterns of the studied materials are shown in Fig. 6. Characteristic peaks of the PP α-phase are observed in the polymer blends and the nanocomposites. For some nanocomposites, a small peak is observed around $2\theta = 20°$. Some authors interpreted this peak as a (130) γ-reflection as a result of the confined PP crystallization in the presence of well dispersed clay [22]. In our case, this peak seems to be rather associated to the presence of clay that exhibits also a peak at the same position (Fig. 6). As shown in Fig. 6, a more pronounced peak at 20° is observed for PP/15A in which poor dispersion is obtained and where a confined crystallization cannot take place between the clay platelets. Although the PP/MA blends and the nanocomposites show the same PP reflections, a significant difference in the intensity of the reflections α_1 (110) and α_2 (040) is observed. Orientation indexes based on the reflection intensities were determined and the values are reported in Table 4. The results show that the values for the A_{hk0} index of the polymer blends and the nanocomposites are not significantly different. In all cases, these values are comprised between 0.71 and 0.80, in agreement with values obtained in the core of PP injected samples [23]. However, significant difference is observed in the A_{040} index. For the nanocomposites, the value of A_{040} is increased by 60% when compared to those of the polymer blends. This indicates some preferential orientation of the PP α-crystallite in the nanocomposites, which is probably related to the orientation of the clay particles induced by the compression molding. It does not however seem to be related to the level of clay dispersion since the A_{040} index for PP/15A with poor clay particles dispersion is higher than for PP/15A/MA9k in which better clay dispersion was observed. Moreover,

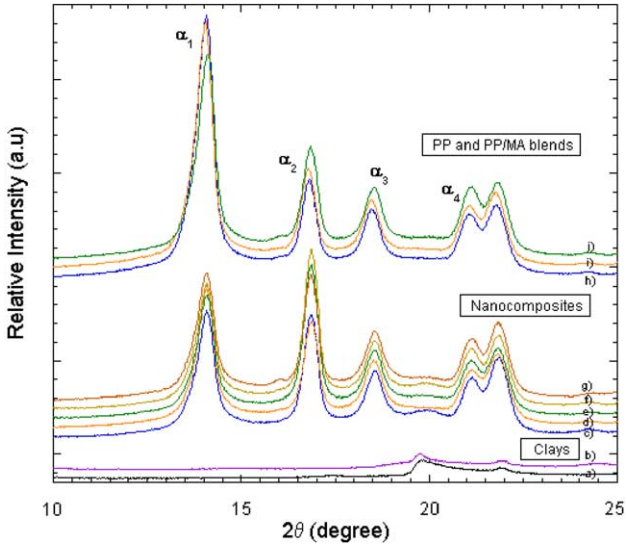

Fig. 6. WAXS patterns of (a) 15A, (b) 30B, (c) PP/15A, (d) PP/15A/MA9k, (e) PP/15A/MA330k, (f) m(PP/15A)/MA330k, (g) m(PP/30B)/MA330k, (h) PP, (i) PP/MA9k and (j) PP/MA330k.

Table 4
Orientation and crystallinity indexes

	Orientation index		Mean crystallite size (nm)	Crystallinity index
	A_{hk0}	A_{040}	L_{040}	$C_i/C_{PP}\times 100$ (%)
PP	0.78	0.22	28.8	100
PP/MA9k	0.78	0.22	31.4	100
PP/MA330k	0.74	0.28	29.0	100
PP/15A	0.71	0.40	28.1	84
PP/15A/MA9k	0.72	0.34	28.7	82
PP/15A/MA330k	0.75	0.47	30.5	88
m(PP/15A)/MA330k	0.74	0.48	31.9	91
m(PP/30B)/MA330k	0.80	0.41	32.6	77

although the A_{040} index is higher in the presence of clay, the value of L_{040}, which reflects the mean crystallite size determined perpendicular to the (040) plane, is similar for both the polymer blends and the nanocomposites (Table 4). This indicates that the presence of clay induces some PP crystallite orientation but with no particular change in the crystallite size. The relative crystallinity index values also reported in Table 4 are found to be higher for the polymer blends than for the nanocomposites. This is in agreement with the fact that the presence of clay does not increase the PP matrix crystallinity.

3.4. Interpretation for the clay dispersion and intercalation process

From the results of this study, scenarios for the mechanisms of clay dispersion and intercalation in the presence of the two coupling agents can be proposed. These scenarios are shown in Fig. 7.

When a coupling agent with a low molecular weight is used, such as MA9k in the present case, the high mobility of its short chains and their high grafting content allow them to interact actively with a large number of clay platelets and a high clay surface area during compounding. This leads to good clay dispersion in PP/15A/MA9k with high sub-micro-level clay density and makes effective clay intercalation easier. In such case, clay platelets collapse and large interlayer spacing distribution effects are thus quite limited. The relative uniformity of the intercalation process in PP/15A/MA9k suggests that only MA9k molecules penetrate between the platelets, otherwise larger degree of intercalation and larger interlayer spacing distribution would be obtained. As a consequence, the platelets distance is limited by the length of the chains of MA9k. Effective intercalation can thus be obtained, but it cannot be enhanced to high clay interlayer spacing. When a coupling agent with a high molecular weight is used, such as MA330k in the present case, the low mobility of its long chains and their low grafting content allow them to interact with a limited number of clay platelets and a low level

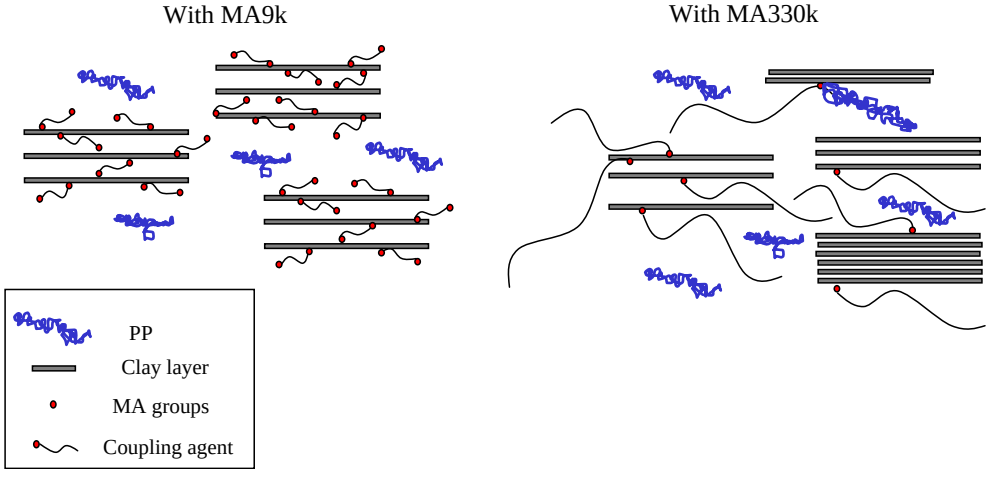

Fig. 7. Scheme of the clay intercalation process with the two MA coupling agents.

of clay surface area. This leads to good clay dispersion in PP/15A/MA330k with high sub-micro-level and also nano-level clay density but with a less uniform intercalation process as compared to PP/15A/MA9k. Because of the long chains of MA330k and its expected better miscibility with the PP matrix that can accommodate for further larger intercalation, the intercalation of this coupling agent leads to an effective and larger platelets distancing as seen by higher clay interlayer spacing in local clay disordered structure. Moreover, it favors a better and finer dispersion. Besides, due to the characteristics of this coupling agent as the low grafting content, limited intercalation still remains. Different extent of intercalation is thus obtained with MA330k, some with higher level compared to MA9k. Mechanisms of clay dispersion and intercalation are also dependent on the type of organo-clay used. Despite the presence of coupling agent in m(PP/30B)/MA330k, coarse clay dispersion with very low sub-micro-level clay density and very limited intercalation occur that could be explained in part by the small interlayer spacing of clay 30B and the low thermal stability of its intercalant.

4. Conclusions

PP nanocomposites using different organo-clays and MA-PP coupling agents were prepared by melt blending. The effect of clays and coupling agents on the nanocomposite micro- and nano-structure in terms of clay dispersion, intercalation and PP crystalline morphology was studied. The results of this study show that:

- The use of MA-PP coupling agent leads to generally intercalated nanocomposites where clay is finely dispersed with high density of sub-micro-level particles and in some case nano-level particles.
- Depending on the characteristics of the MA-PP coupling agent (molecular weight and grafting content), different extent of clay intercalation is reached.
  - The use of MA-PP with a low molecular weight (M_w) and high grafting content leads to relatively good and uniform intercalation ($d_{001} = 3.6$ nm; narrow XRD (001) peak; regularity of the clay interlayer spacing observed in TEM) but with no observed signs of exfoliation. Such MA-PP can interact largely with clay particles and intercalate easily clay platelets. However, the lack of miscibility with the PP matrix can explain why further larger intercalation cannot be achieved.
  - The use of MA-PP with high molecular weight and low grafting content leads to more heterogeneous intercalation ($d_{001} = 3.1$ nm; broad XRD (001) peak; wider range of clay interlayer spacing observed in TEM) with some signs of exfoliation (disordered and more distanced layers structure, small particles of 2 – 3 layers). Such MA-PP can interact to a lesser extent with clay due to its lower grafting content leading to some limited intercalation. However, its higher M_w and better miscibility with PP allows some larger level of intercalation to partial exfoliation to be achieved.
- The fine clay dispersion obtained in the presence of MA-PP leads to a crystallization at lower temperature and at a lower rate but does not affect the level of crystallinity. Further work should be done to study the kinetics of crystallization in such cases.
- The presence of clay, depending on its dispersion, affects the PP morphology, i.e. spherulite size and also induces some PP crystallite orientation.
- The type of clay intercalant can lead to drastic effect on clay dispersion, inducing platelets collapse and clay particles aggregation due to thermal degradation. Thermal stability of the intercalant stays thus still a crucial issue and has to be taken into account in the melt compounding process.

References

[1] Sinha Ray S, Okamoto M. Prog Polym Sci 2003;28:1539.
[2] Alexandre M, Dubois P. Mater Sci Eng 2000;28:1.
[3] Ton-That M-T, Perrin F, Lacand P, Cole KC, Denault J, Enright G. Proceedings of the international symposium on polymer nanocomposites, Montreal Canada, November 14–16 2001.
[4] Kawasumi M, Hasegawa N, Kato M, Usuki A, Okada A. Macromolecules 1997;30:6333.
[5] Kato M, Usuki A, Okada AJ. Appl Polym Sci 1997;66:1781.
[6] Hasegawa N, Kawasumi M, Kato M, Usuki A, Okada A. J Appl Polym Sci 1998;67:87.
[7] Reichert P, Nitz H, Klinke S, Brandsch R, Thomann R, Mulhaupt R. Macromol Mater Eng 2000;(275):8.
[8] Svoboda P, Zeng C, Wang H, Lee LJ, Tomasko DL. J Appl Polym Sci 2002;85:1562.
[9] Maiti P, Nam PH, Okamoto M. Macromolecules 2002;35:2042.
[10] Hambir S, Bulakh N, Jog JP. Polym Eng Sci 2002;(42):800.
[11] Kalgaonkar RA, Jog JP. J Polym Sci, Part B: Polym Phys 2003;(41):3102.
[12] Bassett DC, Olley RH. Polymer 1984;25:935.
[13] Klug HP, Alexander LE. X-ray diffraction procedures for polycrystalline and amorphous materials. NY, USA: Wiley; 1974 pp. 618–708.
[14] Sheng N, Boyce MC, Parks DM, Rutledge GC, Abes JI, Cohen RE. Polymer 2004;45:487.
[15] Trotignon JP, Lebrun JL, Verdu J. Plast Rubber Process Appl 1982;2:247.
[16] Zhu P-W, Edward G. Macromol Mater Eng 2003;288:301.
[17] Bu H-S, Cheng SZD, Wunderlich B. Makromol Chem Rapid Commun 1988;9:75.
[18] Cho K, Li F, Choi J. Polymer 1999;40:1719.
[19] Ton-That MT, Perrin-Sarazin F, Cole KC, Bureau MN, Denault J. Polym Eng Sci 2004;44:1212.
[20] Dermatas D, Dadachov MS. Appl Clay Sci 2003;23:245.
[21] Denault J, Vu-Khanh T. Polym Compos 1988;9:360.
[22] Nam PH, Maiti P, Okamoto M, Kotaka T, Hasegawa N, Usuki A. Polymer 2001;42:9633.
[23] Trotignon JP, Verdu J. J Appl Polym Sci 1987;34:1.